Responses to Referee #2's comments

The manuscript presents an automatic algorithm for horizontal ice crystal (HOIC) identification using the combination of the attenuated backscatter and volume depolarization ratio of HOICs for zenith and 15°-off-zenith lidar measurements. Moreover, using Doppler radar measurements, the authors provide insights of the physical processes in clouds with HOICs.

In general, the work is well-presented and the results seem quite promising towards the identification of HOICs and the description of the physical processes. There are though several aspects that require more attention, as for example the points highlighted from Referee #1. In addition, a more appropriate characterization of the lidar measurements should be provided. Since the algorithm is heavily based on the volume depolarization ratio measurements from the zenith (MPL) and off-zenith (AVORS) lidars, more details need to be provided regarding the calibration procedure and the uncertainties of the volume depolarization measurements:

Reply: We sincerely thank Referee #2 for reviewing our paper and providing constructive comments for improvement. Responses to these comments are provided below. In this author's comment, we reply (in blue font) to Referee #1's comments (in black font and key points in red font). The relevant part in the revised version is in green font.

Revisions regarding lidar calibration:

1. Since the identification algorithm is heavily-based on the values of the volume depolarization ratio measured at zenith with MPL lidar and at 15°-off-zenith with AVORS lidar, the calibration of these systems should have been done following higher standards than the comparison with a reference system. For example, why the procedures according to established lidar networks (e.g. EARLINET) or the extensive work of Freudenthaler (2016) were not followed?

Reply:

In principle, we should use the best calibration method for the depolarization calibration. The accurate depolarization is the first step for an identification method using the depolarization ratio. We did the calibration at the beginning of our research.

However, the two lidars, MPL and AVORS, used here are compact and commercial, small-sized lidars. The height of both lidars is below one meter (see Fig. S4). For this reason, an adaptation of the system to perform $\Delta 90$ calibrations, as described by Freudenthaler (2016), has not been possible.

The reference Raman lidar is relatively large and is wrapped inside a container. For this system the $\Delta 90$ depolarization calibration procedure is conducted regularly to confirm the validity of the depolarization ratio. The depolarization performance of this Raman lidar has also been validated by another collocated high spectral resolution lidar (HSRL) (Wang et al., 2022). In general, it is a reliable lidar as a reference system.

For such compact systems, the calibration using a reference system has shown promising results (Córdoba-Jabonero et al. 2021; Papetta et al. 2024). Papetta et al. (2024) introduced an empirical method to perform this type of calibration, which allows to consider changes in the

inter-channel gain ratio factor and also polarization effects in the system. We followed this approach and were able to match the depolarization ratio of the three systems, i.e., the calibrated Raman system, and the two compact systems (MPL and AVORS). In the case of the MPL the same detector is used to measure the co and cross polarized components keeping the gain factor over time stable, and the comparison of the MPL and AVORS system in the molecular region in the long term corroborates the stability of the AVORS's gain ratio as well.

We added the description in the revised manuscript, Line 500-501:

"Since the MPL and AVORS lidar are both compact, small-sized lidars, the standard $\Delta 90$ method (Freudenthaler 2016) is not applicable."

2. As shown in Fig. B1c and d, the "MPL-calibrated" and "AVORS-calibrated" volume depolarization ratios show differences with the reference Raman lidar, that indicate possible limitations in the calibration procedure used. In addition, Fig. B2 shows the differences for the volume depolarization ratio when both lidars measure at the zenith direction. The authors should justify the differences, providing an analysis for the cases associated with the larger ones shown in the plots (especially in Fig. B2). Moreover, in line 478 the authors refer to the differences shown in Fig. B1 as "acceptable": First, the authors need to provide the uncertainties of volume depolarization ratio profiles for all three lidars (MPL, AVORS, Raman), and include them in the plots. Then, they need to provide the larger differences that are "acceptable" for the algorithm presented, and discuss whether the differences shown in Fig. B1 and B2 are smaller than these thresholds.

Reply:

- For the Fig. B1c, the main difference is from the calibrated MPL and Raman lidar depolarization ratio below 2 km. The difference is about 1%. Within 2 km, there is always an effect of overlap calibration uncertainty which affects the depolarization ratio for Raman lidar and AVORS lidar (but not in MPL because it only has one optical path), and it usually can not be solved 100%. There could also be deadtime effects for MPL in the near range that might deviate a bit the depolarization.
- In Fig. B1d, the depolarization ratios measured by the MPL and Raman lidars are nearly identical, with a maximum difference of approximately 2%. However, the AVORS lidar, operating at a 15-degree off-zenith angle, exhibits a higher depolarization ratio within the ice cloud layer, likely due to the presence of horizontally oriented ice crystals, compounded by spatial heterogeneity. These oriented crystals may significantly enhance the depolarization signal in AVORS measurements compared to the zenith-pointing MPL. Additionally, the differing fields of view (FOV)—0.1 mrad for MPL and 0.2 mrad for AVORS—contribute to slightly distinct multiple scattering effects within dense clouds, further amplifying the observed differences.

- Provide analysis in Figure B2 difference

The results of the depolarization calibration, both before and after, are shown in Fig. S1 using density scatterplots.

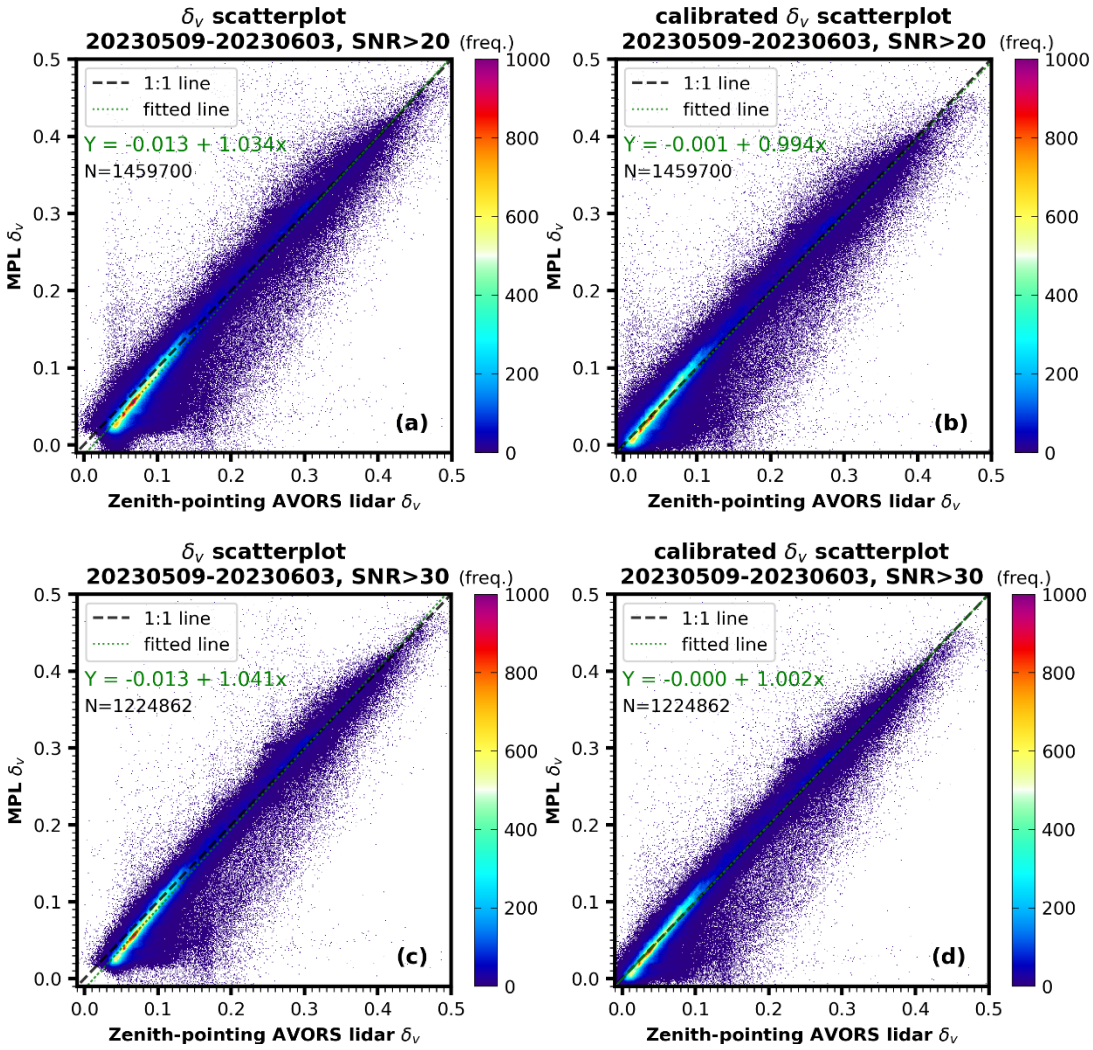

Figure S1. Density scatterplots of depolarization ratio (δ_v) before (a, c) and after (b, d) depolarization calibration for MPL and zenith-pointing AVORS lidar from 9 May 2023 to 3 June 2023, when two lidars were both zenith-pointing. Data include clouds, aerosols, and molecules with signal-to-noise ratios greater than 20 (a, b) or 30 (c, d). The 1:1 line and least-squares regression fits are shown for comparison.

From Fig. S1, it is evident that the consistency between the depolarization measurements of the two lidars improved significantly after calibration. The intercept of the least squares fit becomes closer to zero following the calibration. However, since the calibration is a linear transformation, it cannot remove the noisy points that deviate from the 1:1 line. As the AVORS lidar was positioned outside the container, it was more susceptible to solar noise, resulting in a lower signal-to-noise ratio (SNR). This may also contribute to the observed discrepancies. By increasing the SNR threshold from 20 to 30 for point selection, we observed a better agreement in the calibrated depolarization ratio (compare Fig. S1b and S1d).

A representative case was observed on 21 May 2023, featuring multiple ice cloud layers and a dust layer, which highlights the effectiveness of the calibrated lidar depolarization

measurements (Fig. S2). The two zenith-pointing lidars show excellent agreement across both high and low depolarization regions throughout the 0–14 km observation range.

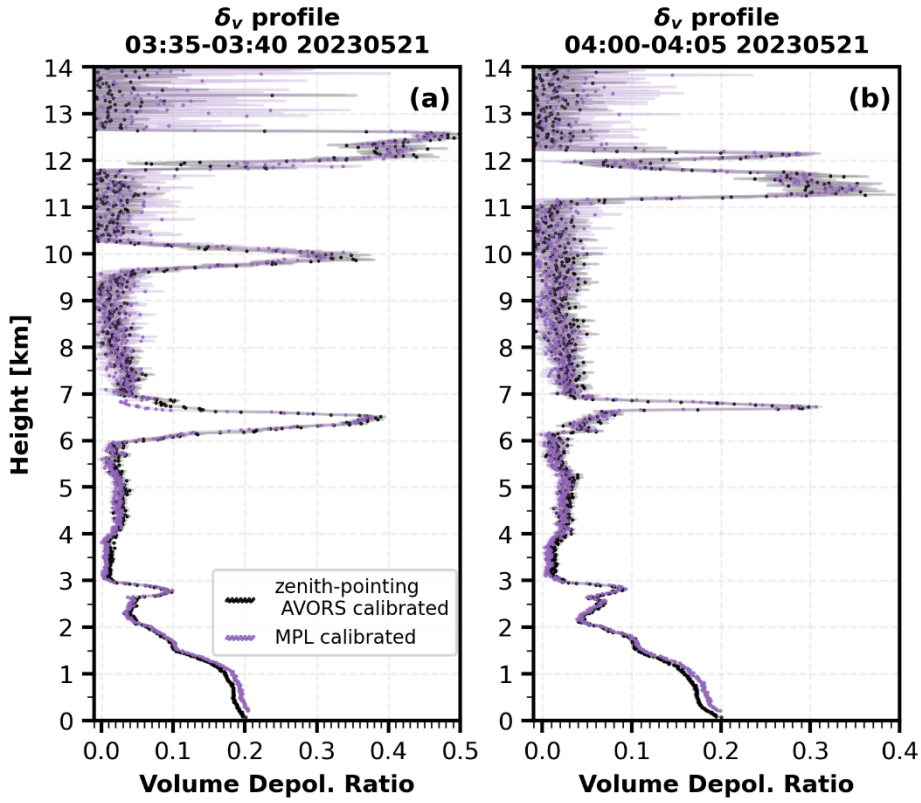

Figure S2 The zenith-pointing MPL and zenith-pointing AVORS lidar volume depolarization ratio profiles on 21 May 2023, (a) 03:35-03:40 and (b) 04:00-04:05, Local Time. The shaded error bar areas correspond to the uncertainty for depolarization calculation and calibration.

- One case with a large difference:

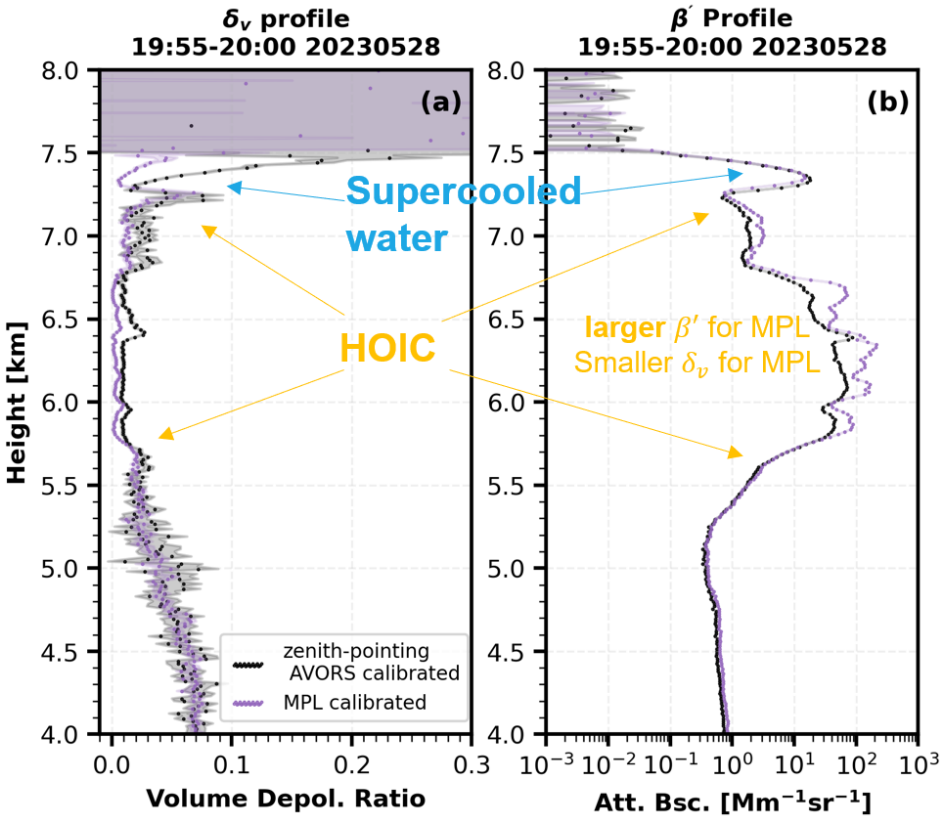

Figure S3 The zenith-pointing MPL and zenith-pointing AVORS lidar volume depolarization ratio profiles (a) and attenuated backscatter profiles (b) on 28 May 2023, 19:55-20:00, Local Time. The shaded error bar areas correspond to the uncertainty for depolarization ratio and attenuated backscatter, respectively.

A case exhibiting a significant difference in depolarization ratio was observed on 28 May 2023, involving supercooled liquid water (~7.8 km), horizontally oriented ice crystals (HOICs, 5.8–7 km), and an aerosol layer (below 5 km), as shown in Fig. S3.

A continuous geometrically thick region of low depolarization ratio with high backscatter indicates the presence of HOICs. The depolarization ratio profiles from both lidars show good agreement, except in the regions associated with HOICs and the supercooled liquid water cloud above. The MPL lidar exhibits a lower depolarization ratio within the supercooled liquid water cloud due to its smaller field of view (FOV) and reduced multiple scattering effects. Interestingly, the MPL also shows a lower depolarization ratio in the HOIC region.

Upon examining the attenuated backscatter profiles, we found that the MPL shows a higher backscatter signal within the HOIC region, while the backscatter profiles of MPL and AVORS are nearly identical in the supercooled liquid water and other regions. This suggests that the observed depolarization difference in the HOIC region is likely due to a slight off-zenith pointing of the AVORS lidar during this case. The AVORS lidar may not be ***perfectly*** zenith-pointing at the time.

The MPL was located inside a vertical container and equipped with a vertical length hood to ensure strict zenith-pointing alignment (see Fig. S4). The potential maximum off-zenith angle

θ of the MPL is estimated using Eq. (1) based on the geometrical relationships illustrated in Fig. S4c and S4e.

$$\theta = \arctan\left(\frac{0.17/2}{3}\right) = 1^{\circ}14' \quad (1)$$

Based on the geometrical calculation shown in Eq. (1), the potential maximum off-zenith angle of the MPL is estimated to be approximately 1° ***at most***, although it is typically well aligned with the zenith direction (see Fig. S4d and S4e). In contrast, the AVORS lidar was positioned outdoors, where it is more difficult to ensure ***exact 90-degree zenith-pointing***. It is therefore possible that a slight off-zenith angle existed during this observation period. This minor misalignment may explain the observed depolarization ratio discrepancies in the HOIC region.

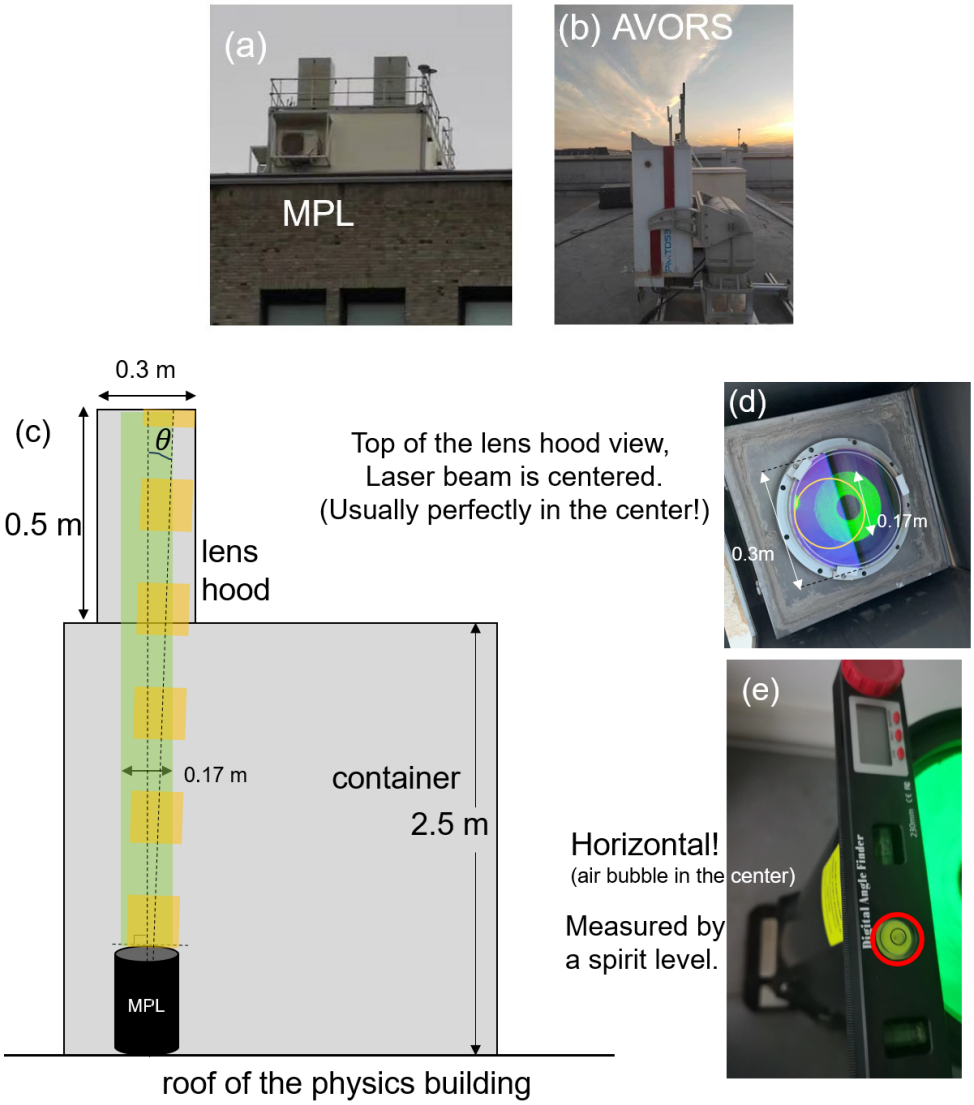

Figure S4 Appearance of the MPL container (a) and the AVORS lidar system (b). (c) Schematic diagram of the MPL container. (d) Top view of the lens hood and (e) spirit level measurement at the upper edge of the MPL, demonstrating the precise zenith-pointing alignment of the MPL system.

➢ Provide the uncertainties of volume depolarization ratio profiles. Add them in the plots.

The uncertainties in the volume depolarization ratio were generally estimated using error propagation formulas. In the figures, these uncertainties are illustrated as shaded regions. The methods used to calculate uncertainties for different systems are described below:

Raman lidar:

The signal of the channels is glued from the photon counting and analog signals. The uncertainties are estimated from the Poisson distribution and the Monte Carlo simulation. Subsequently, the overall uncertainty of the depolarization ratio is derived using error propagation from the individual uncertainties of each channel.

MPL:

The final uncertainty of MPL depolarization ratio is calculated as Eq. (2):

$$\Delta\delta_{\text{calibrated}} = \sqrt{(\Delta\delta_{\text{MPL}})^2 + (\Delta_{\text{offset}})^2} \tag{2}$$

Here, $\Delta\delta_{\text{MPL}}$ represents the uncertainty of the uncalibrated MPL depolarization ratio, which is derived using an error propagation approach similar to that described by Heese et al. (2010). The uncertainties of the individual channels are first estimated based on Poisson statistics, and then propagated to obtain $\Delta\delta_{\text{MPL}}$.

The term Δ_{offset} refers to the uncertainty of the applied offset during calibration. It is derived from the intercept uncertainty obtained via least-squares fitting between the MPL and the reference Raman lidar depolarization ratios, as summarized in Table 1.

AVORS lidar:

The depolarization ratio uncertainty of AVORS lidar is calculated using Eq. (D1) from Papetta et al. (2024). Here we denote as Eq. (3).

$$(\Delta\delta)^2 = \left[\left(\frac{\Delta P^{\perp}}{P^{\perp}}\right)^2 + \left(\frac{\Delta P^{\parallel}}{P^{\parallel}}\right)^2 + \left(\frac{\Delta K^*}{K^*}\right)^2\right]\left(\frac{P^{\perp}}{P^{\parallel}K^*}\right)^2 + (\Delta g\,)^2 \tag{3}$$

Figure S5 is the updated Fig. B1 with uncertainties in the revised manuscript.

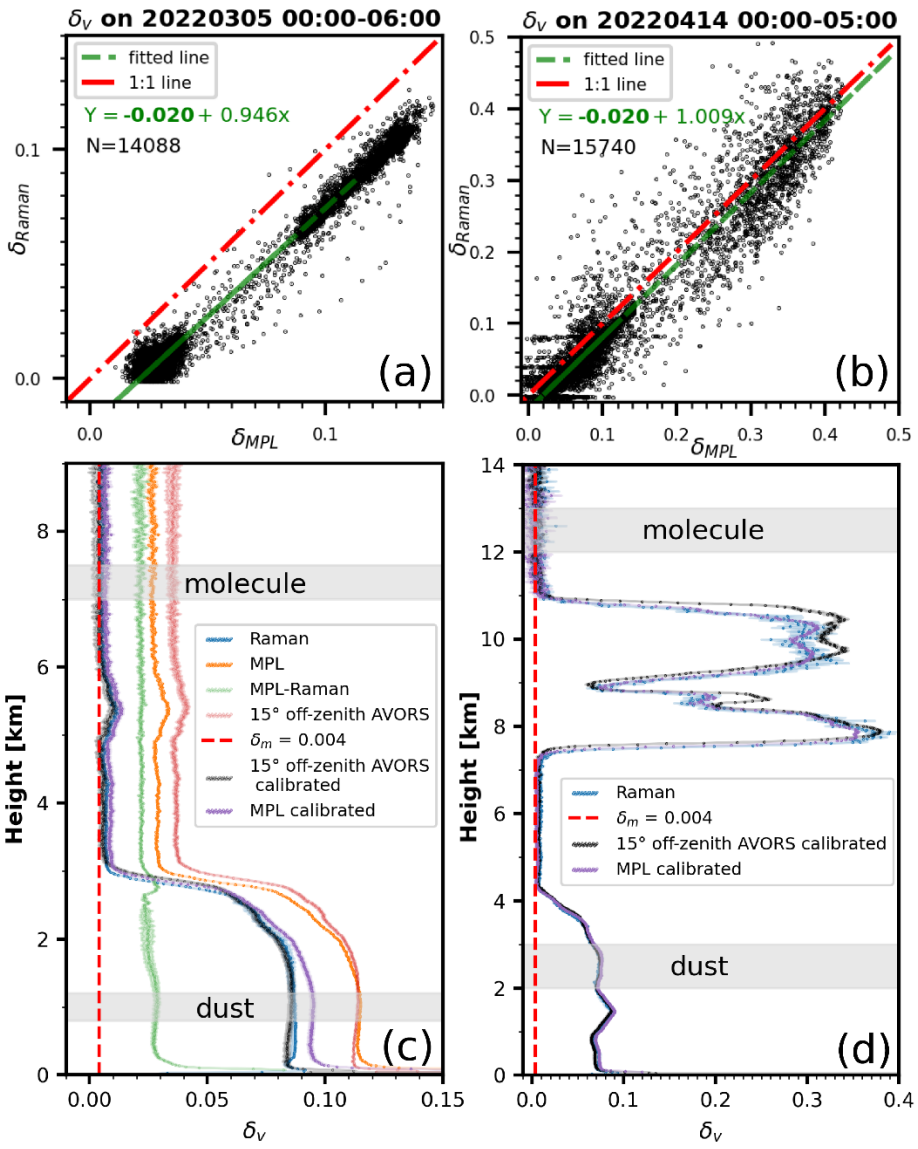

Figure S5 Scatter plot of well-calibrated Raman lidar and MPL uncalibrated depolarization ratio on (a) 5 March 2022, 00:00-06:00, Local Time and (b) 14 April 2022, 00:00-05:00, Local Time; (c) Averaged Depolarization profiles on 5 March 2022, 0:00-06:00; (d) Averaged Depolarization profiles on 14 April 2022, 00:00-05:00; The horizontal gray shaded areas indicate the reference ranges used for dust and molecular layers. The shaded regions around the lines represent the uncertainties associated with depolarization ratio calculation and calibration.

- Discuss the “acceptable”.

As shown in Fig. S5(c), Fig. S6(c), and Fig. S2, the depolarization ratio of the calibrated MPL is occasionally slightly higher than that of the AVORS lidar. However, the region below 2 km, where this difference is most pronounced, is generally unimportant for identifying horizontally oriented ice crystals (HOICs). Therefore, the imperfect performance of the calibrated depolarization ratio in this layer has minimal impact on HOIC detection.

The primary low-altitude difference is that the MPL generally exhibits higher depolarization ratios than AVORS. However, in cases of strong specular reflection, as illustrated in this study (Fig. 5b)—the MPL shows significantly lower depolarization ratios compared to the off-zenith AVORS lidar. Based on our observations, the MPL depolarization ratio can perfectly approach zero for strong backscattering targets such as liquid water clouds and HOICs. The main low-altitude bias in the MPL depolarization ratio appears in intermediate backscatter targets, such as dust layers, which are out of this study's focus.

Figures 5b and S3a demonstrate that the MPL performs well in HOIC identification, exhibiting near-zero depolarization values in HOIC-dominated regions. Importantly, the applied constant offset of 2% cannot be increased further, as doing so would result in negative depolarization ratio values in low-depolarization regions—an unphysical outcome.

Compared with previous studies such as Westbrook et al. (2010), our work represents a step forward by employing the same wavelength with depolarization measurement capabilities. Based on our experience, even when using two identical lidar systems (i.e., same model, wavelength, field of view, and detector) to observe the same target (aerosols or clouds), differences in measured depolarization ratios can still occur. These discrepancies may result from system complexity, random noise, or minor imperfections in hardware performance.

To evaluate the robustness of the separation criterion (threshold of 0.6 for the ratio of zenith to off-zenith depolarization) used in the classification flowchart (Fig. 2), we conducted a sensitivity analysis. We tested the influence of uncertainties in the depolarization ratio of the zenith and off-zenith pointing lidars using the long-term values from range bins identified as ice-containing clouds (including mixed-phase clouds and ROICs). The depolarization uncertainties range between 5-10 % (percentual error, according to Figs. S2, S5c, and S6c) for the two systems. These ranges keep the rate of falsely identified HOICs and ROICs below 2 – 5%, corroborating the tolerance of the classification scheme to uncertainties in the depolarization. For this reason, we consider the underlying uncertainties acceptable.

The discussion has been added in the revised manuscript, Line 513-515:

"From our observation, the region below 2 km, where this difference is most pronounced, is generally unimportant for identifying HOICs (in the 13 October 2022 case, HOICs are above 4 km). Therefore, the imperfect performance of the calibrated depolarization ratio in this layer has minimal impact on HOIC detection."

And add the sensitivity test result at Line 550-554:

"Sensitivity tests were performed to evaluate the stability of the 0.6 threshold (ratio of zenith to off-zenith depolarization) used in the classification flowchart (Fig. 2). Assuming typical depolarization uncertainties (5–10%, percentual error) as shown in Fig. B1, the analysis based on long-term statistics of ice-containing clouds indicates that the percentage of falsely identified HOICs and ROICs below 2-5%, which corroborates the tolerance of the classification scheme to uncertainties in the depolarization."

3. MPL lidar calibration: The volume depolarization ratio provided by the MPL lidar is compared with the corresponding measurements from the reference Raman lidar, showing an

offset in MPL data. Then, the MPL-calibrated volume depolarization values are derived from subtracting this offset. It is not clear if this offset is constant in time –in the manuscript we see that it does not change within a month. Moreover, as mentioned by the authors, the reference Raman lidar system does not operate continuously. Provide a brief description of the number of the available reference measurements used for the calibration of MPL lidar during the 1-year of measurements discussed in the manuscript (do the same for the AVORS lidar –point (3)).

Reply:

Available reference measurements:

The available Raman lidar data are limited to the first five months of 2022 (January to May), totaling five months. After 12 May 2022, the instrument ceased functioning due to a failure.

An ideal case for calibrating the MPL depolarization ratio involves a prolonged period of uniform dust layers coinciding with an aerosol-free region during nighttime. The presence of ice clouds above is preferable, as this study focuses on ice crystals; however, such optimal cases are rare in our observations.

For the off-zenith-pointing AVORS lidar, ice cloud cases require careful selection. Potential horizontally oriented ice crystals and heterogeneity may result in a calibrated volume depolarization ratio within the cloud that differs slightly from those of the zenith-pointing MPL or Raman lidar.

Córdoba-Jabonero et al. (2021) utilized an aerosol-free case from June 29–30, 2019, to calibrate their depolarization ratio.

In this study, we selected the cases of February 26, March 5, April 14, and May 7, 2022 (see Figs. B1 and S6), to determine a 2% offset for the MPL depolarization calibration. These same cases (February 26, March 5, April 14, and May 7, 2022) were also used to derive the parameters K^* and g for the AVORS lidar.

The corresponding text is added or revised to the revised manuscript, Line 507-509 and Line 536-540:

"Additional cases (not shown here) from 00:00 to 01:00 on 26 February 2022 and from 00:00 to 05:00 on 7 May 2022 further validate the consistency of the -0.02 offset."

"Three additional cases—00:00–01:00 on February 26, 2022; 00:00–05:00 on April 14, 2022; and 00:00–05:00 on May 7, 2022—were selected using a consistent method involving molecule and dust regions to derive robust K^* and g values. The resulting K^* and g values are presented in Fig. B2 with statistics. Ultimately, we obtained $K^* = 0.962 \pm 0.006$ and $g = 0.0327 \pm 0.0009$. The calibrated depolarization ratio profile was calculated from Eq. (B3) using the robust K^* and g."

- Discuss the offset of 2% is constant in time.

The last case presented in Appendix B2 is the one from 14 April 2022. To demonstrate the temporal stability of the 2% depolarization ratio offset, we selected the earliest available Raman lidar observation from February 2022 (data quality in January was insufficient) and the

latest available case from May 2022. Two additional cases used in the depolarization calibration (26 February and 7 May 2022) are shown in Fig. S6. As shown in Fig. S6 and Table 1, the 2% offset remains consistent over time. After May 2022, Raman lidar data became unavailable. However, the MPL system was not physically moved after that time, and the internal temperature of the MPL container was kept stable using air conditioning. Furthermore, the calibrated MPL and AVORS lidars showed excellent agreement on 21 May 2023, over one year later. Based on these factors, we confidently assume that the 2% offset remains valid after May 2022.

In addition, we tested the two-parameter calibration method proposed by Papetta et al. (2024), which introduces an additional factor K^* to improve calibration accuracy. While this method yielded near-perfect results for the calibration case, it exhibited signs of overfitting and did not perform well for other cases. Consequently, we opted to retain the simpler, constant 2% offset approach.

It is worth noting that the depolarization ratio difference between the MPL and the reference Raman lidar was not entirely uniform across range. A slightly larger discrepancy was observed below 2 km, where the MPL tended to report higher depolarization ratios. We attribute this either to differences in the overlap of the polarization channels in the reference Raman system, or to near-range effects in the MPL, such as the deadtime effect. However, this height range is not critical for our study, as HOIC (horizontally oriented ice crystals) occurrences below 2 km are extremely rare—in this study, all were observed above 4 km.

Importantly, we could not increase the offset beyond 2%, as the molecular scattering region already yields a depolarization ratio close to 0.0004. A larger offset would result in negative depolarization values in this region, which is physically implausible. Additionally, the specular reflection region in Fig. 5b shows depolarization values only slightly above zero; applying a larger offset would drive these values into the negative, which would again be unphysical. For these reasons, we maintained the 2% offset throughout the study.

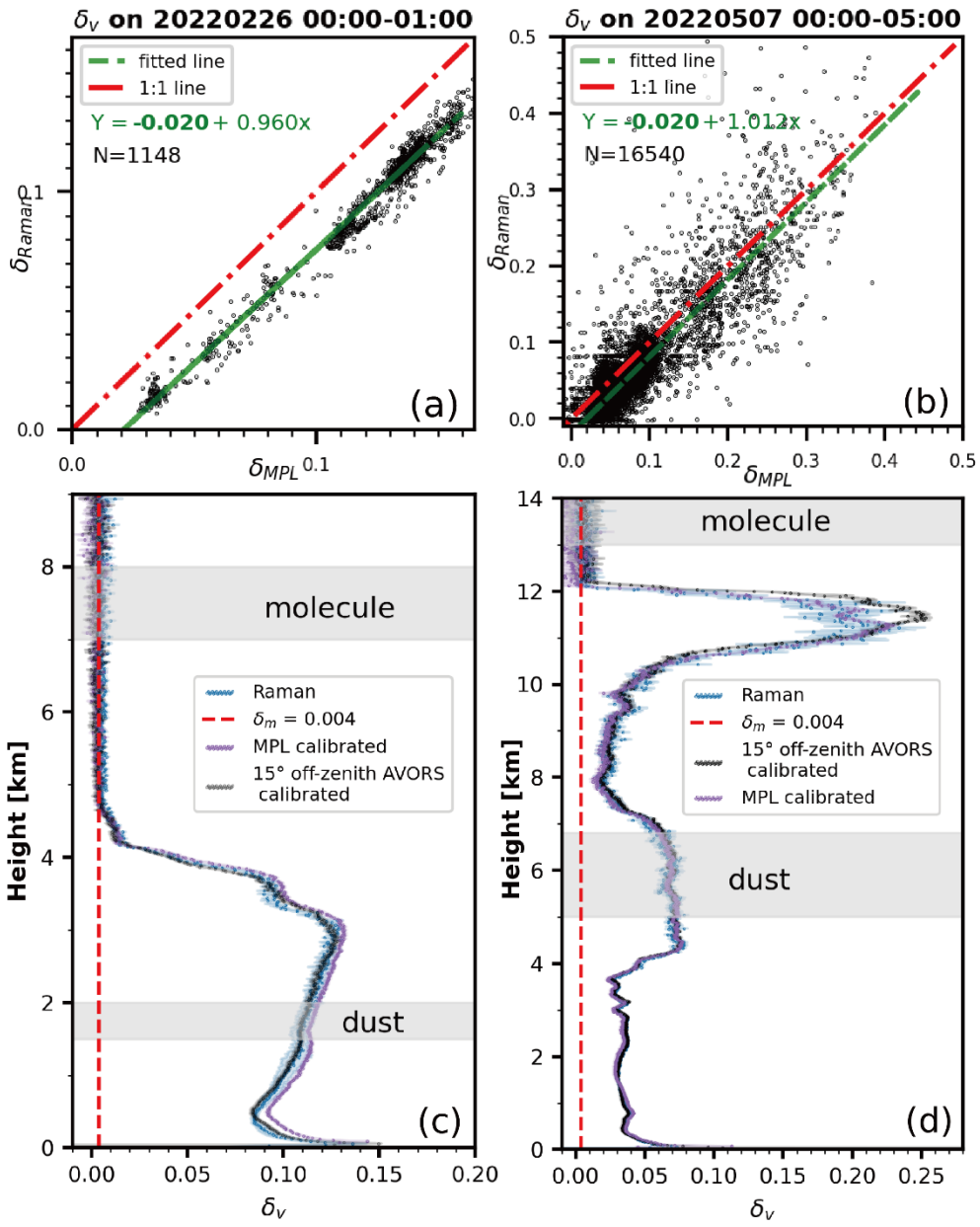

Figure S6 Scatter plot of well-calibrated Raman lidar and MPL uncalibrated depolarization ratio on (a) 26 February 2022, 00:00-01:00, Local Time and (b) 07 May 2022, 00:00-05:00, Local Time; (c) Averaged Depolarization profiles on 26 February 2022, 0:00-01:00; (d) Averaged Depolarization profiles on 07 May 2022, 00:00-05:00; The horizontal grey shade regions indicate the reference ranges used for dust and molecular layers. The shaded error bar areas correspond to the uncertainty for depolarization calculation and calibration.

The 2% offset, derived from the intercept of the least-squares fit, is based on precise values reported in Table 1, yielding a final average offset of -0.02011 ± 0.00101."

Table 1. Average intercept of the least-squares fit for each examined period with the standard deviations.

Date	20220226	20220305	20220414	20220507	average
offset	-0.02030 ±0.00051	-0.02015 ± 0.00006	-0.02003 ±0.00220	-0.01999 ±0.00336	-0.02011 ±0.00101

4. AVORS lidar calibration: Provide brief statistics on K* and g, for all reference measurements (from Raman lidar) used to characterize the AVORS lidar depolarization calibration, similar to what is presented in Fig. 7 of Papetta et al. (2024).

Reply:

Thank you for pointing this out! We evaluated four different cases, resulting in updated values of *K** and *g*, as presented in Table 2 and Fig. S7. The values of *K** and *g* were revised from 0.954 and 0.0329 to 0.962 and 0.0327, respectively. All figures related to depolarization were redrawn using these updated parameters. The calibrated depolarization ratio exhibits only minor changes with the revised *K** and *g*.

Figure S7 has been added to the manuscript as new Fig. B2.

The derived *K** and *g* values are relatively stable compared to the highly variable cases presented in Fig. 7 of Papetta et al. (2024). In their study, the Cimel lidar under calibration and the reference Raman lidar were separated by tens of kilometers rather than co-located, which likely contributes to the greater variability observed in *K** and *g*.

Table 2. Average polarization parameters for each examined period are given with the standard deviation.

Date	20220226	20220305	20220414	20220507	average
*K**	0.9649 ± 0.0036	0.9545 ± 0.0029	0.9675 ± 0.0045	0.9618 ± 0.0043	0.9622 ± 0.0062
g	0.0312 ± 0.0002	0.0329 ± 0.0002	0.0330 ± 0.0002	0.0337 ± 0.0003	0.0327 ± 0.0009

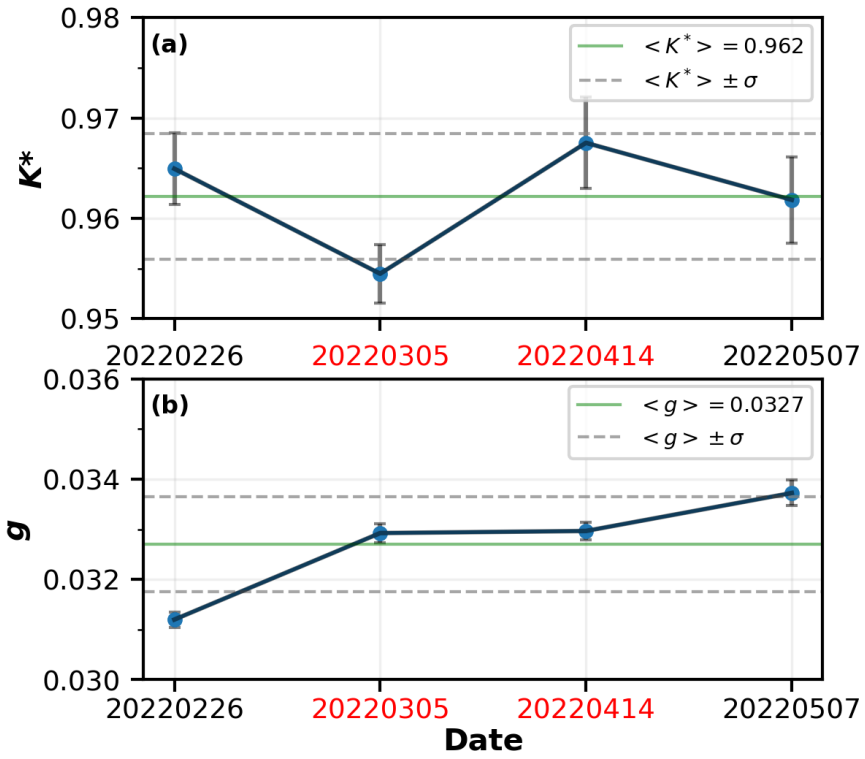

Figure S7 Temporal evolution of polarization parameters derived using the two-parameter approach. Error bars indicate the variability of the derived parameters within the selected molecular scattering and dust reference layers. The average polarization parameter value and its standard deviation in the whole period is shown by solid green lines and dashed gray lines, respectively. The timestamps of the cases shown in Fig. B1 are highlighted in red.

Other revisions:

Line 68: Replace “Passive satellite” with “Passive satellites”.

Reply: Done!

Line 206: Replace “If by contrast, the above δoff-zenith > 0.1 ice-containing cloud pixels show δzenith < 0.1…” with “If the cloud parts categorized as ROICs or MCPs have δoff-zenith > 0.1 and δzenith < 0.1…”.

Reply: Done!

Line 208: Replace “…i.e.…” with “…since.…”

Reply: Done!

Lines 209-210: Replace “…kept their ROIC or MPC labels.” with “categorized as ROIC or MPC.”

Reply: Done!

Line 214: “The threshold values were fixed empirically from the whole cloud dataset collected during 2022.” And lines 226-230 “For the identification scheme, … for specular reflection.” Support these empirically-derived values with values provided in the literature from lidar measurements and scattering calculations of ROICs and HOICs.

Reply: I have added some literature as follows.

0.1 and 0.3 are frequently used criteria for liquid droplet and ice crystal discrimination. In principle, liquid water droplets show a low depolarization ratio, and ice crystals show a high depolarization ratio. The criteria of 0.3 are quite common for ice crystal identification. Due to the strong multiple scattering effect from liquid water clouds, the criterion of liquid water droplets is not exactly zero but slightly larger than zero. Since different fields of view contribute to different scales of multiple scattering. Here, the criteria of 0.1 are determined from long-term observation (> 0℃).

2 and 0.6 are simply statistical results from the long-term yearlong dataset (see Fig. 3b). We assume that most of the cloud range bins are ROIC-dominant and not strongly affected by the HOICs. And the upper left branch of Fig. 3b is are HOIC dominant region. They are new criteria, so we do not have literature to support them.

The relevant literature has been added in the revise manuscript Line 220-221:

“(Seifert 2011; Lewis et al. 2020; Whitehead et al., 2024)”

Lines 330-334: “Figure 7 shows … where HOICs exist.” Provide possible reasons why this happens. Is there a possibility that the results shown in Fig. 7 are biased due to the attenuation of the lidar signals, which may result to non-identification of HOICs at higher heights and lower temperatures? Discuss.

Reply: Thank you for pointing out this! We added sentences to try to explain the results, Line 339-340 and Line 343-344:

“Higher temperatures (-8>*T*>-22 °C) favor the formation of plate-like ice crystals, while weaker horizontal winds exert less torque to disturb their quasi-horizontal orientation.”

“Overall, in the troposphere, higher altitudes are associated with lower temperatures and stronger horizontal winds—a pattern that also applies to regions where HOICs are present.”

We added a discussion part after the sentence, Line 344-349. Ground-based lidar-based cloud research always has this defect from lidar attenuation.

“It should be noted that the non-detection of HOICs at higher altitudes due to lidar signal attenuation may introduce a slight bias in the results, potentially leading to an overestimation of temperature and an underestimation of horizontal wind speed. This limitation is common in ground-based lidar studies of clouds. However, based on radar observations indicating a cloud top height of approximately 7 km and radiosonde data showing a minimum temperature above −22 °C and maximum horizontal wind speeds below 25 ms^{-1}, the overall bias is expected to be minor. Therefore, the main conclusions of this study remain robust.”

Line 336: Replace “…spectral with…” with “…spectral width…”.

Reply: Done!

Lines 349-350: "Contrary … as shown in Fig. 4(l)." Provide possible reasons.

Reply: The LDR of plate-like ice crystals is too small. The current sensitivity of cloud radar cannot detect it. We have added, Line 365-366:

"This is likely because the LDR of plate-like ice crystals is too small for the current sensitivity of cloud radar to detect."

Line 434: Replace "…are require help…" with "….are required to help…"

Reply: Done!

Lines 457-459: Replace "The photo count rate … laser energy." with corresponding equation.

Reply: Thank you for pointing this out! I added the corresponding equation after the sentence:

"The above steps are summarized as the Eqs. B1 and B2:

$$\mathrm{NRB_{MPL}} = \frac{[(Photo\ Count\ Rate \times Dead\ Time\ Correction) - Afterpluse - Background] \times range^2}{Overlap \times Laser\ Energy} \quad \text{(B1)}$$

$$\mathrm{NRB_{AVORS}} = \frac{[(Photo\ Count\ Rate \times Dead\ Time\ Correction) - Background] \times range^2}{Overlap \times Laser\ Energy} \quad \text{(B2)}$$

Line 498: Replace "…Fig. 2c." with "…Fig. B1c."

Reply: Done!

References:

Córdoba-Jabonero, C., Ansmann, A., Jiménez, C., Baars, H., López-Cayuela, M.-Á., and Engelmann, R.: Experimental assessment of a micro-pulse lidar system in comparison with reference lidar measurements for aerosol optical properties retrieval, Atmospheric Measurement Techniques, 14, 5225–5239, https://doi.org/10.5194/amt-14-5225-2021, 2021.

Freudenthaler, V.: About the effects of polarising optics on lidar signals and the Δ90 calibration, Atmos. Meas. Tech., 9, 4181–4255, https://doi.org/10.5194/amt-9-4181-2016, 2016.

Heese, B., Flentje, H., Althausen, D., Ansmann, A., and Frey, S.: Ceilometer lidar comparison: backscatter coefficient retrieval and signal-to-noise ratio determination, Atmos. Meas. Tech., 3, 1763–1770, https://doi.org/10.5194/amt-3-1763-2010, 2010.

Lewis, J. R., Campbell, J. R., Stewart, S. A., Tan, I., Welton, E. J., and Lolli, S.: Determining cloud thermodynamic phase from the polarized Micro Pulse Lidar, Atmos. Meas. Tech., 13, 6901–6913, https://doi.org/10.5194/amt-13-6901-2020, 2020.

Papetta, A., Marenco, F., Kezoudi, M., Mamouri, R.-E., Nisantzi, A., Baars, H., Popovici, I. E., Goloub, P., Victori, S., and Sciare, J.: Lidar depolarization characterization using a reference system, Atmospheric Measurement Techniques, 17, 1721–1738, https://doi.org/10.5194/amt-17-1721-2024, 2024

Seifert, P.: Dust-related ice formation in the troposphere: A statistical analysis based on 11 years of lidar observations of aerosols and clouds over Leipzig, PhD thesis, University of Leipzig, Leipzig, Germany, https://nbn-resolving.org/urn:nbn:de:bsz:15-qucosa-71167, 2011

Wang, N., Zhang, K., Shen, X., Wang, Y., Li, J., Li, C., ... & Liu, D. Dual-field-of-view high-spectral-resolution lidar: Simultaneous profiling of aerosol and water cloud to study aerosol–cloud interaction. Proceedings of the National Academy of Sciences, 119(10), e2110756119. https://doi.org/10.1073/pnas.2110756119, 2022

Westbrook, C., Illingworth, A., O'Connor, E., and Hogan, R.: Doppler lidar measurements of oriented planar ice crystals falling from supercooled and glaciated layer clouds, Quarterly Journal of the Royal Meteorological Society, 136, 260–276, https://doi.org/10.1002/qj.528, 2010.

Whitehead, L. E., McDonald, A. J., and Guyot, A.: Supercooled liquid water cloud classification using lidar backscatter peak properties, Atmos. Meas. Tech., 17, 5765–5784, https://doi.org/10.5194/amt-17-5765-2024, 2024.